LARGE EDDY SIMULATION OF SHOCK WAVE/TURBULENT BOUNDARY LAYER INTERACTION AT M=2.25

Abdellah Hadjadj, Samuel Dubos, Guillaume Ribert

Institut National des Sciences Appliquées de Rouen
CORIA - Unité Mixte de Recherche C.N.R.S. 6614
Avenue de l'Université, BP 8
76801 Saint Etienne du Rouvray, France
hadjadj@coria.fr

ABSTRACT

This work deals with numerical simulation of supersonic turbulent flows when shock/turbulent boundary layer interaction occurs. Such flows reveal the existence of complex mechanisms, which have to be well understood for an efficient design of propulsion systems. In this study, large eddy simulation is used to investigate unsteady mechanisms. Since a shock-capturing scheme is used, an hybrid numerical scheme has been developed to reduce its dissipative properties. The issue of the generation of coherent turbulent boundary conditions is also addressed. A method originally developed by Lund, based on a rescaling technique, has been modified by adjusting the scaling coefficient to provide smooth transition between the inner and the outer parts of the boundary layer. This modification is essential for avoiding the drift previously observed in the mean streamwise velocity profile. The obtained results are analysed and discussed in terms of mean and turbulent quantities. Excellent agreement between LES, DNS and experimental data is obtained. Especially, oscillations of the reflected shock occurring at low frequencies are observed, in agreement with experimental investigations. Moreover, simulations reveal the presence of such frequencies inside the recirculation bubble. This point gives credit to the hypothesis which presents the instabilities of the reflected shock as a consequence of the dynamic properties of the separated zone.

INTRODUCTION

Eddy structures and internal dynamics of supersonic turbulent boundary layers may play an important role in aerospace applications, specifically when surface heat transfer on high-speed vehicles or unsteadiness in shock/turbulent boundary layer interactions are of concern (see Fig. 1).

Today, large-eddy simulation has demonstrated its capabilities in calculations of relatively complex flows and can be used as a design tool for real-time optimization. The rising computational power and the improved numerical techniques are able to solve more scales presented in turbulent flows and thus predicting unsteady effects better than RANS or URANS methods. The purpose of this paper is to develop reliable CFD tools and estimate the area of their applicability for complex compressible flows situations, including shocks, boundary layer, acoustics, compressibility effects... The primary focus of the present contribution is the study of a spatially-developing turbulent boundary layer at Mach number 2.5 over an adiabatic flat plate with and without shock interaction using LES method. This problem has been experimentally investigated by Deleuze (1995), Laurent (1996) and Dupont et al. (2005). In addition, analyses of the turbulent structures and shock/boundary layer unsteadiness may significantly contribute to the understanding of the turbulence behaviour of supersonic boundary layers as well as the development of improved compressible turbulence models.

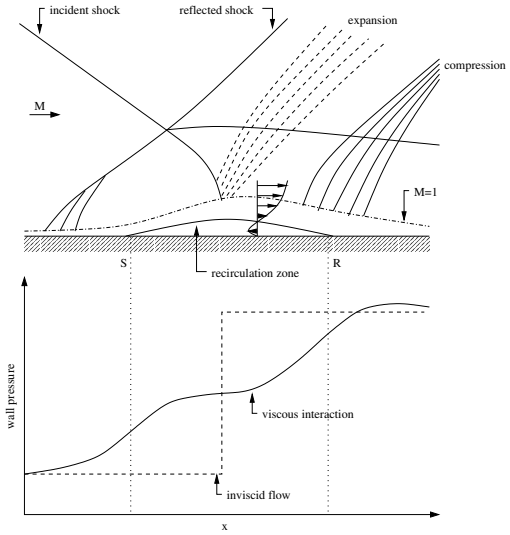

Figure 1: Schematic illustration of shock/turbulent boundary layer interaction and surface pressure distribution.

NUMERICAL PROCEDURE AND LES METHODOLOGY

In addition to sub-grid scales modeling, another issue of LES technique is the choice of the numerical method. As pointed out by Ghosal (1996), Kravchenko and Moin (1996), the truncation error of low-order schemes may exceed the SGS term, leading to a high numerical damping. Moreover, when fully compressible flows are investigated, pressure (or density) discontinuities may appear and have to be captured without adding too much numerical viscosity. To achieve this goal, a fifth-order WENO solver (Jiang, 1996) combined with a centred fourth-order scheme is used to calculate the convective fluxes. In addition, a selective Ducros' sensor is employed to confine the use of the WENO scheme to the portions of the flow that contain discontinuities (shocks). This technique contributes to reduce significantly the numerical dissipation introduced by the "upwinding" of shock-capturing schemes. Viscous terms are discritized using a centred fourth-order accurate, while an explicit third-order Runge-Kutta of Shu and Os-

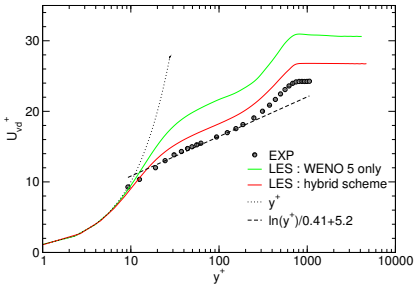

Figure 2: Influence of numerical scheme on the normalized longitudinal velocity profile (with $U^+_{vd} = \int_0^{U^+} \sqrt{\rho/\rho_p}\, dU^+(y^+) = ln(y^+)/\kappa + C$).

her (1988) is used for time integration. For numerical stability reasons, the minimum value of Ducros' sensor Φ (where $\Phi = (div\,(\vec{u}))^2/(rot\,(\vec{u}))^2 + (div\,(\vec{u}))^2$), for which the centred scheme is selected, is fixed to $\Phi_c = 0.035$. The computed mean value of Φ shows that the centred scheme is mainly used within the boundary layer. The advantage of using a hybrid scheme is evident from Fig. 2, where the normalised mean velocity profile U^+_{vd} exhibits a better behaviour. In particular, if only the WENO scheme is used, the value of the skin-friction velocity, u_τ, is underestimated by approximately 30% compared to experimental data. However, this underestimation is reduced to ∼10% with the hybrid scheme, which is customary for compressible LES as previously reported on Syropoulos (1998) and Sagaut (2004). Concerning the inflow boundary conditions, an existing method of generation of unsteady compressible turbulent boundary layers (Lund et al., 1998, Urbin et al., 1999 and Stolz et al., 2004) has been modified to avoid the drift of the mean velocity profile, observed in supersonic boundary layer simulations. The modification was achieved through an appropriate adjustment of the scaling coefficient to provide smooth transition between the inner and the outer parts of the boundary layer (Dubos, 2004). Doing so, the new recycling and rescaling method becomes robust and relaxes faster towards the target experimental values (mainly the skin-friction velocity, $u_\tau = \tau_w^{1/2}$, where $\tau_w = \nu(\partial u/\partial y)|_w$ and the boundary-layer thickness δ). In the present study, the dynamic model of Germano and Lilly (1991) has been employed for modeling the small-scale turbulence.

RESULTS AND DISCUSSION

Supersonic incoming boundary layer

A numerical investigation of a supersonic incoming boundary layer at $M_\infty = 2.3$ and $R_{e_\theta} = 5000$ (in the absence of interacting shock) is first reported here. This test-case provides the (unsteady) inflow conditions to the shock-boundary layer interaction problem. The size of the computational domain is: $L_x \approx 15\,\delta$, $L_y \approx 6.5\,\delta$ and $L_z \approx 0.6\,\delta$, where $\delta = 10.83\,mm$ is the incoming boundary-layer thinckness. Notice that the spanwise length of the computational domain represents $1/10^{th}$ of the experimental wind tunnel extent. The two-point autocorrelation coefficients in the homogeneous direction (z), for both the turbulent velocity and thermal variables, are examined. Results (not presented here for concision) show that the decorrelation of velocity fluctuations is achieved over a distance of $L_z/2$, indicating that the computational domain is chosen large enough to not inhibit

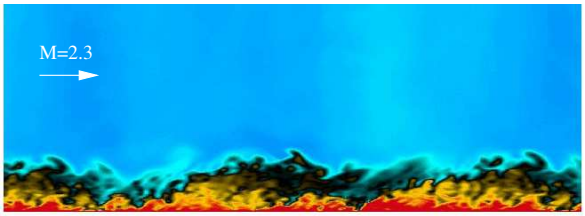

Figure 3: Instantaneous temperature field (boundary layer without incident shock).

the turbulence dynamics. The mesh has about 2.4×10^6 grid points, distributed in wall units as: $\Delta x^+ = 40$, $\Delta z^+ = 7$ and $\Delta y^+_{min} = 1$, where $y^+ = yu_\tau/\nu_w$, with ν_w and ρ_w the kinematic viscosity and the density at the wall, respectively. These computations were performed on a parallel IBM-SP Power4 using 40 processors and required 140h of CPU time.

Figure 4: Instantaneous longitudinal velocity fluctuations in a wall-parallel plane at $y^+ \approx 10$.

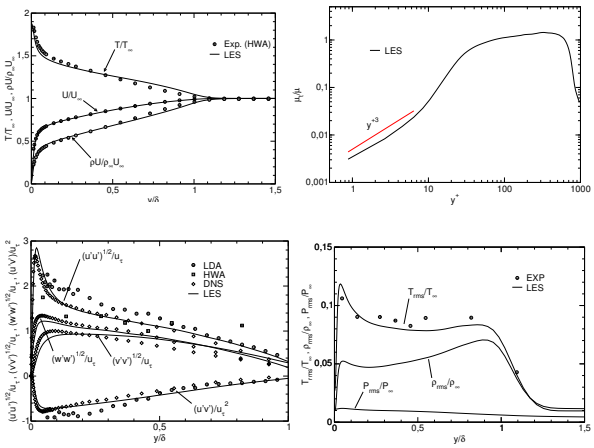

Figure 5: Distributions of normalized mean flow variables, sub-grid turbulent viscosity, normalized Reynolds shear stresses and r.m.s values as function of y/δ.

An unsteady view of the supersonic flow is presented in Fig. 3. The examination of the instantaneous three-dimensional iso-vorticity field shows that the boundary layer is fully developed and self preserving. Also, the simulation reveals the appearance of large-scale motion in the outer region of the boundary layer, dominated by the entrainment process. These large-scale structures are particularly active near the boundary-layer edge, where they remain coherent long enough and are strongly responsible for the intermittency of the boundary layer its growth rate. Near-wall streaks can be visualized by contours of the streamwise velocity fluctuation, which is shown in Fig. 4 in a wall-parallel plane at $y^+ \sim 10$. It is obvious from Fig. 4 that the computational domain contains several streaks (more than 5) in the spanwise direction, spaced by about $L_z^+ = 455$ wall units, which is 4 times larger than the "Minimal Flow Unit"recommended by Jimenez & Moin (1991). The reported turbulence statistics are examined to evaluate their consistency with both DNS (Pirozzoli et al., 2004) and experimental measurements (Deleuze, 1995 and Laurent, 1996). They are based on time-averaging

of the instantaneous three-dimensional fields that were extracted from a time series covering 160 characteristic times $\tau_m = \delta_i/U_\infty$, where δ_i is the incoming boundary-layer thikness evolving at a free-stream velocity, U_∞. As shown in Fig. 5, simulations match well with experimental results (see Dubos for other parameters of interest).

Shock/boundary-layer interaction

The second part of this paper concerns the shock-boundary layer interaction, studied experimentally by Deleuse (1995) and Laurent (1996) at IUSTI, Marseille. The compression corner has an angle of incidence of $\theta = 8°$, corresponding to an oblique choc with 32.41° of inclination at $M_\infty = 2.3$.

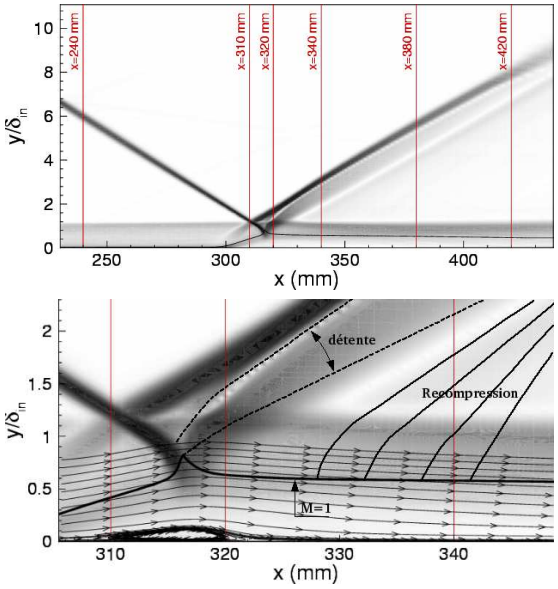

Figure 6: Numerical schlieren pictures of the shock/boundary layer interaction, computated using the mean density field. ___ : sonic ligne.

The incoming boundary condition is extracted from previous data of spatially-developping boundary layer. The size of the computational domain is nearly the same, except an extension made in both x and y directions to cover all the interaction zone as well as the relaxation region and to ovoid a possible confinement of the shock system in the spanwise direction. The mesh contains $N_x \times N_y \times N_z = 312 \times 160 \times 65$ points. The computations were performed on a parallel IBM-SP4 using 25 processors and required 2800h of CPU. It is important to notice that the presence of shock-wave poses a particular problem in LES. Indeed, the sub-grid viscosity ratio, μ_t/μ, may exhibit high values near discontinuities, even outside the boundary layer where the flow is not turbulent. This result is not surprising since the amount of sub-grid viscosity evolves proportionally to the second invariant of the deformation tensor. Thus, a turbulence crossing a shock can be artificially amplified by too much sub-grid viscosity. To avoid this problem, the sub-grid model was used only in the portions of the flow where the fourth-order centred scheme was active, *i.e.* $\mu_t = 0$ if WENO scheme was used.

Instantaneous structure and mean properties

Fig. 6 shows the mean turbulent flow structure, with an induced separation shock and a reversed flow. On the back of the incident shock wave, which penetrates up to the sonic line, the appearance of an expansion fan followed by a compression shock help the boundary layer to reattach the wall and relax further downstream. The instantaneous density field, reported in Fig. 7, reveals the existence of complex organized motion in the outer part of the boundar layer, which is characterized by the occurrence of large scale structures that exhibit intermittent character. The incident shock bends toward the wall while entering the boundary layer, and a small recirculation bubble is observed near the wall. The computed average of surface pressure, skin friction coefficient, mean and fluctuating velocities, turbulent shear-stress and mean temperature distributions at several measurement planes are shown in Figs. 8-12. The computation shows close agreement with experiment.

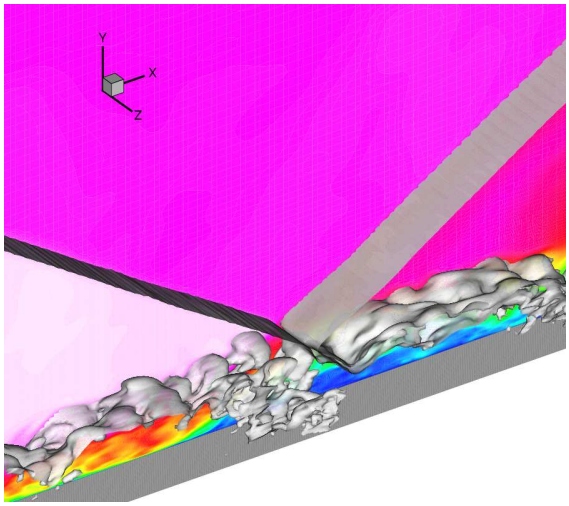

Figure 7: Enlargement of the shock/boundary layer interaction zone, (iso-density contours).

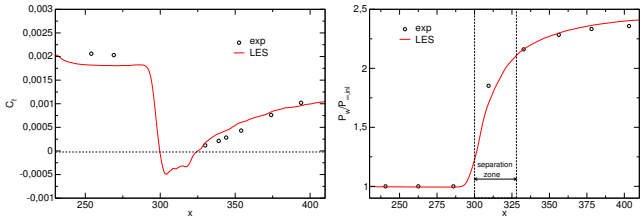

Figure 8: Average skin friction coefficient (left) and normalized wall pressure distribution (right).

Strong Reynolds Analogy

In supersonic turbulent flows, the Strong Reynolds Analogy (SRA) is derived from the assumptions that the total temperature fluctuations are negligible, and the Prandtl number is one, which leads to the following relation:

$$SRA = \frac{\sqrt{\overline{T'T'}}/\widetilde{T}}{(\gamma-1)\bar{M}^2\sqrt{\overline{u'u'}}/\widetilde{u}} \approx 1 \qquad (1)$$

where $\bar{M} = \bar{u}/\bar{c}$ is the local Mach number. Relation (1) implies that velocity and temperature fluctuations are anti-correlated, i.e., their correlation coefficient is:

$$R_{u'T'} = \frac{\overline{u'T'}}{\sqrt{\overline{u'^2}\;\overline{T'^2}}} \approx -1 \qquad (2)$$

As shown in Fig. 13, the relation (1) is valid in the whole boundary layer and over all the region of the interaction.

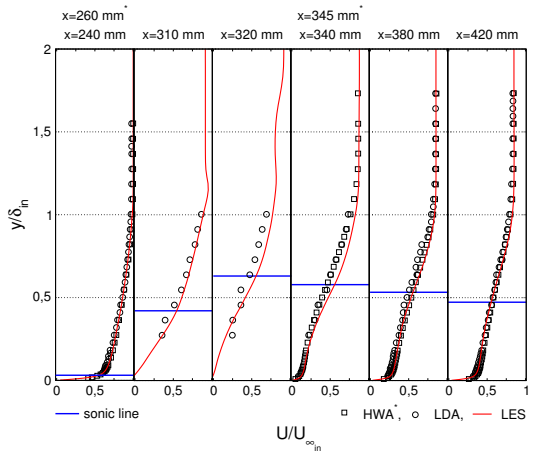

Figure 9: Longitudinal mean velocity.

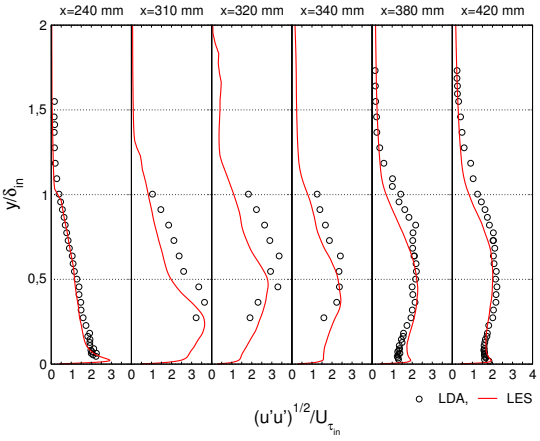

Figure 10: Longitudinal fluctuating velocity.

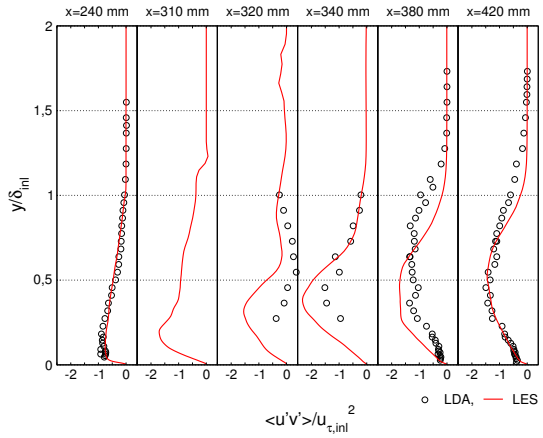

Figure 11: *Turbulent shear stress* $\overline{u'v'}$.

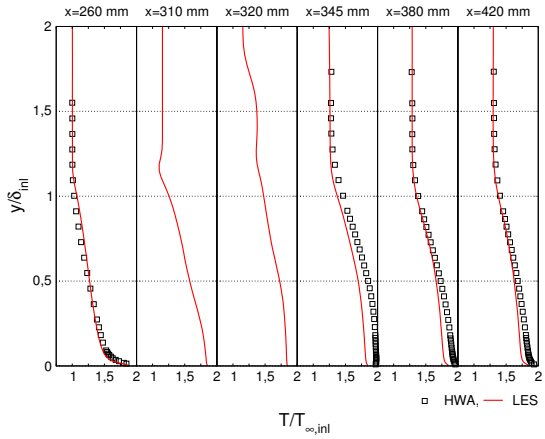

Figure 12: *Mean temperature distributions.*

However, as reported in Fig. 14, the value of the measured correlation coefficient $-R_{u'T'}$ is less than unit (≈ 0.8). Recent DNS of supersonic boundary layer (Pirozzoli et al., 2004 and Guarini et al. 2000) have shown that this coefficient fails to 0.60 throughout most of the boundary layer and exhibits a maximum value of 0.84 when the wall is approached. DNS and LES reproduce the same trend. As suggested by Gaviglio (1987), discrepancies between experiments and simulations may be due to a difference in the magnitude of the acoustic field which is much lower in the computations than in blowdown supersonic wind tunnels. Of course, this hypothesis needs to be further investigated, in particular the role of acoustic waves in the reduction of $R_{u'T'}$ correlation has yet to be studied and understood.

Analysis of SWBLI unsteadiness

Unsteadiness of shock/boundray-layer inteactions is known to be a crucial issue for wall loads, especially those encountered in rocket nozzles. This problem is mainly related to the large-scale boundary structures that convect into the shock from upstream, and that is connected with the instantaneous behavior of the separated zone. Fig. 15 displays contours of r.m.s pressure, $\sqrt{\overline{p'p'}}$, in all the computational domain. Amplification of pressure fluctuations is much more important in the interaction zone and in the downstream relaxation region (8% to 9% of $P_{\infty,inl}$) compared to the upstream BL, which exhibits a lower level (2% of $P_{\infty,inl}$). This behavior is clearly visible on the wall pressure distribution, reported in Fig. 16, showing strong values of $\sqrt{\overline{p'p'}}$ around the reflected shock. In accordance with recent experimental observations (Dupont et al., 2005), one can think that this amplification is due to the unsteadiness behavior of the separation shock system. In the same way, the foot of the incident shock, supported by the sonic line, exhibits a strong fluctuations, which possibly result from oscillations of the recirculation bubble, being reflected on the sonic line.

Power Spectral Density (PSD) of wall pressure fluctuations is shown in Fig. 17. The colored field represents spatial distribution of iso-PSD (x, $log(F)$) normalized by its local integral, $G_N(F)$. This normalization has the advantage to better highlight the contribution of each frequency at a given coordinate x, with: $\int_0^\infty G_n(f)df\big|_x = 1$. The average wall pressure profile is also reported on Fig. 17 to help localization of compression waves acting on the shock foot. An energy accumulation at low frequencies is observed at $x = 295mm$ and $x = 310mm$ (including a part of the separated zone), which reveals the existence of a low frequency movement of the reflected shock ($< 1kHz$ and $St = 0.019$). This observation is in agreement with experimental investigations, which emphasize a dominant frequency, associated with the shock movement, of $400Hz$ ($St = 0.008$). It is worth noticing that the highest energy contribution is located at the beginning of the separation zone ($295mm < x < 300mm$), whereas energies associated with frequencies lower than $1kHz$ are very weak in the upstream BL as well as in the center part

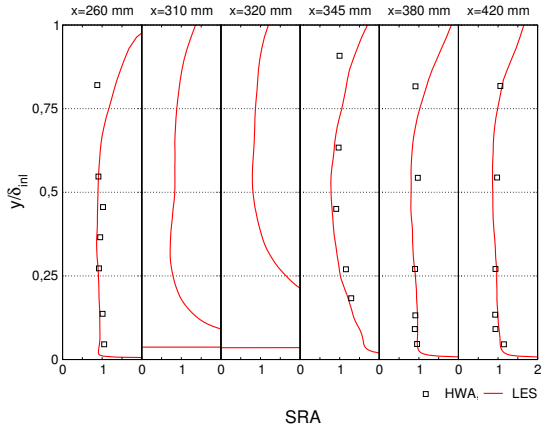

Figure 13: *Plot of the Strong Reynolds Analogy versus y/δ.*

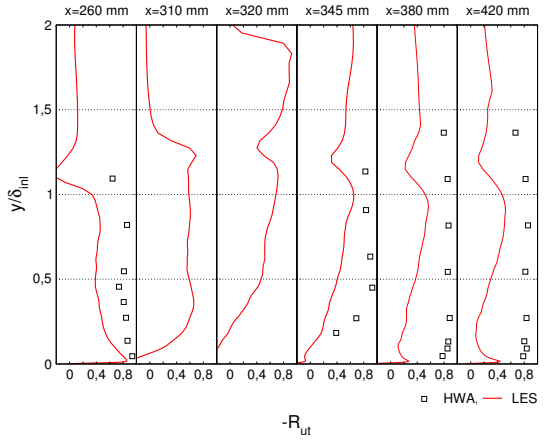

Figure 14: *Plot of the $-R_{ut}$ correlation versus y/δ.*

of the recirculation zone ($x = 315mm$). It seems however that low frequency phenomena reappear at the end of the recirculation zone ($x = 320mm$).

For further investigations of shock oscillations, DSP of surface pressure fluctuations, recorded on the average shock position, at the outer part of the boundary layer ($x = 322mm$ and $y = 16.8mm$, for $y^+_{inl} = 1150$), are presented in Fig. 18. Results show clearly that high energies are associated with frequencies lower than $1kHz$, confirming experimental evidence of low frequencies shock oscillations. On Fig. 18, one can also notice the presence of secondary frequencies of $3kHz$ ($St = 0.058$), $6kHz$ ($St = 0.0117$) and $10kHz$ ($St = 0.114$), very close to the upstream BL frequencies.

Power spectral density signals of $(\rho U)'$ are presented in Fig. 19. Again, one can notice an energy accumulation associated with a low-frequency unsteadiness of the recirculation bubble ($< 1kHz$), featuring similarities with the movement of the reflected shock.

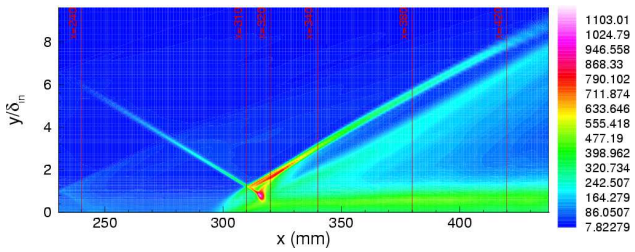

Figure 15: *Plot of $\sqrt{\overline{p'p'}}$ (Pa).*

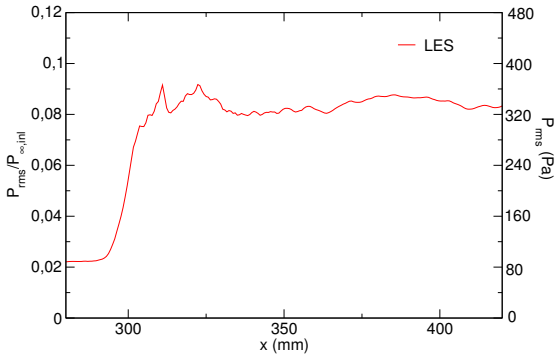

Figure 16: Longitudinal distribution of wall pressure fluctuations.

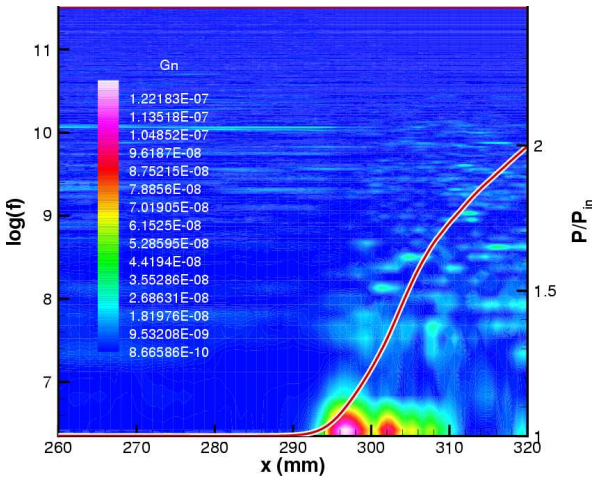

Figure 17: *Power Spectral Density (PSD) of wall pressure fluctuations plotted with the mean profile of wall pressure. PSD normalized using its local integral (s).*

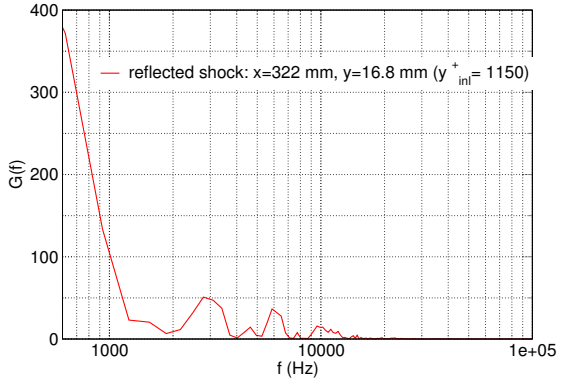

Figure 18: *Power Spectral Density (PSD) of static pressure fluctuations based on the mean incident shock position, near the outer part of the boundary layer (Pa^2/Hz).*

CONCLUSIONS

In this paper, a new approach, based on the use of a combined filter and discontinuity sensor for monitoring the flow solution, is developed and validated for the simulation of supersonic turbulent flows containing shocks with fine scale flow structures. The current research is motivated by

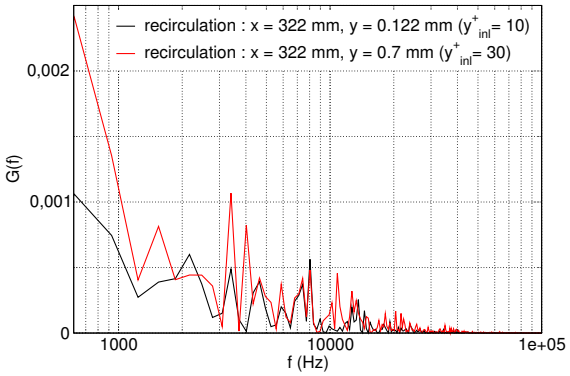

Figure 19: *Power Spectral Density of* $(\rho u)'$ *inside the recirculation bubble* (kgm^{-2}).

the desire to construct reliable compressible Navier-Stokes solvers with accurate numerical tools for predicting complex supersonic aerodynamics in real applications. The numerical procedure, developed in this study (a 3D compressible LES solver with improved inflow-data generation method) has been used to analyse the spatial evolution of a supersonic turbulent boundary layer at M=2.25 with and without shock interaction, studied experimentally by Deleuze (1995) and Laurent (1996). Distributions of mean and turbulent flow quantities are analysed and compared to experimental measurements and DNS data. Very interesting results are obtained. In particular, it is found that the LES accurately predicts the mean temperature and density profiles, skin friction, root mean square of velocity, temperature fluctuations and Reynolds shear stress profiles. In agreement with DNS of boundary layer (in absence of shock), this study shows that the u velocity component and temperature are weakly anti-correlated ($-R_{uT}$ is approximately 0.45). Experimental evidence, however, suggests a higher value of the correlation coefficient than was found in this simulation. This remark holds true for the case of shock-boundary layer interaction. For both cases, fluctuations of the total temperature are not negligible and the strong Reynolds analogy (SRA) is not valid. Finally, oscillations of the reflected shock occurring at low frequencies are observed, in agreement with experimental investigations. Simulations reveal the presence of such frequencies inside the recirculation bubble. This point gives credit to the hypothesis which presents the instabilities of the reflected shock as a consequence of the dynamic properties of the separated zone.

ACKNOWLEDGEMENTS

Part of this work has been carried out within the research activities of the ATAC group (Aérodynamique des Tuyères et Arrière-Corps) supported by CNES and ONERA. Computational facilities were provided by CNRS - IDRIS (Institut du Développement et des Ressources en Informatique Scientifique, Paris).

REFERENCES

Dubos, S., 2005, "Simulation des grandes échelles d'écoulements turbulents supersoniques", Ph.D thesis, INSA of Rouen.

Dupont, P., Haddad, C., Ardissone, J.-P., and Debiève, J.-F., 2005, "Space and time organisation of a shock wave/turbulent boundary layer interaction", *Aero. Sci. Technology*, Vol. 9, pp. 561-572.

Pirozzoli, S., Grasso, F. and Gatski, T. B., 2004, "Direct numerical simulation and analysis of a spatially evolving supersonic turbulent boundary layer at M=2.25", *Phys. Fluids*, Vol. 16, pp. 530-545.

Ghosal, S., 1996, "An analysis of numerical errors in large eddy simulations of turbulence", *J. Comp. Phys.*, Vol. 125, pp. 187-206.

Kravchenko, A. G., Moin P., 1996, "On the effect of numerical errors in large eddy simulations of turbulent flows", *J. Comp. Phys.*, Vol. 131, pp. 310-322.

Jiang, G. S., Shu, C. W., 1996, "Efficient implementation of weighted ENO schemes", *J. Comp. Phys.*, Vol. 126, pp. 202-228.

Shu, C. W., Osher, S., 1988, "Efficient implementation of essentially non-oscillatory shock capturing schemes", *J. Comp. Phys.*, Vol. 77, pp. 439-471.

Pirozzoli, S., Grasso, F., Gatski, T. B., 2004, "Direct numerical simulation and analysis of a spatially evolving supersonic turbulent boundary layer at M=2.25", *Phys. Fluids*, Vol. 16, pp. 530-545.

Guarini, S., Moser, R., Shariff K., Wray, A., 2000, "Direct numerical simulation of a supersonic turbulent boundary layer at Mach 2.5", *J. Fluid Mech.*, Vol. 414, pp. 1-33.

Gaviglio, J., 1987, "Reynolds analogies and experimental study of heat transfert in the supersonic boundary layer", *Int. J. Heat Mass Transfer*, Vol. 30, pp. 911-926.

Stolz, S., Adams, N. A., 2003, "Large-eddy simulation of high-Reynolds-number supersonic boundary layers using the approximate deconvolution model and a rescaling and recycling technique", *Phys. Fluids*, Vol. 15, pp. 2398-2412.

Urbin, G., Knight, D., 1999, "Compressible large eddy simulation using unstructured grid: supersonic boundary layer", *Second AFOSR Conference on DNS/LES, Kluwer Academic Publishers, June 7-9 Rutgers University*, pp. 443-458.

Lund, T. S., Wu, X., Squires, K. D., 1998, "Generation of turbulent inflow data for spatially-developping boundary layer simulations", *J. Comput. Phys.*, Vol. 140, pp. 233-258.

Deleuze, L., 1995, "Structure d'une couche limite turbulente soumise à une onde de choc incidente", Ph.D thesis, Université Aix-Marseille II, France.

Laurent, H., 1996, "Turbulence d'une interaction onde de choc/couche limite sur une paroi plane adiabatique ou chauffée", Ph.D thesis, Université Aix-Marseille II, France.

Spyropoulos, E. T., Blaisdell, G. A., 1998, "Large-eddy simulation of a spatially evolving supersonic turbulent boundary-layer flow", *AIAA J.*, Vol. 36, pp. 1983-1990.

Germano, M., Piomelli, U., Moin, P. Cabot, W.H., 1991, "A dynamic subgrid-scale eddy viscosity model", *Phys. Fluids*, Vol. 3, pp. 1760-1765.

Lilly, D.K., 1991, "A proposed modification of the Germano subgrid-scale closure method", *Phys. Fluids*, Vol. 3, pp. 633-635.

Sagaut P., Garnier E., Tromeur E., Larcheveque L., Labourasse E., 2004, "Turbulent inflow conditions for large-eddy simulation of compressible wall-bounded flows", *AIAA J.*, Vol. 42, pp. 469-477.

Jimenéz, J. and Moin P., 1991, "The minimal flow unit in near-wall turbulence", *J. Fluid Mech.*, Vol. 225, pp.213-240.